ISSN: 2277-9655
(I2OR), Publication Impact Factor: 3.785

IJESRT

INTERNATIONAL JOURNAL OF ENGINEERING SCIENCES & RESEARCH TECHNOLOGY

NEW-FANGLED ASSIMILATION OF A PV-WIND ENERGY SYSTEM WITH ENHANCED EFFICIENCY

Y Heman*, Dr M Sushama
Assistant Professor, Adams Engineering College, Palvoncha, India
Professor, EEE Deprartment, JNTUHCEH, Hyderabad, India

DOI: 10.5281/zenodo.46977

ABSTRACT

A novel integration scheme of solar photovoltaic (PV) with a large capacity doubly excited induction generator-based wind energy system is described. The proposed scheme uses both the grid- and rotor-side power converters of doubly fed induction generator to inject PV power into the grid. Thus, it renders a cost-effective solution to PV-grid integration by obviating the need for a dedicated converter for PV power processing.

The system is able to feed significantly large PV power into the grid compared to an equivalent rating inverter used in the conventional PV-grid system. The proposed scheme prevents circulating power during subsynchronous operation during the availability of solar radiation. All these features enhance system efficiency. System stability is also augmented due to turbine inertia, facilitating high PV penetration into the power grid. The intermittent but complementary nature of solar PV and wind energy sources considerably improves the converters' utilization. Besides, the proposed scheme does not hamper maximum power point tracking of PV and wind sources except during very rarely occurring environmental glitches, which the PV power control algorithm is suitably geared to handle. A comprehensive system model is presented and used for designing the control strategy. The proposed scheme is supported by analysis, simulations, and experiments on a laboratory prototype.

KEYWORDS: Converter control, dc–ac converter, doubly fed induction machine, hybrid system,maximum power point tracking (MPPT), solar photovoltaic (PV), wind generation.

INTRODUCTION

INCREASING industrialization, growing population, and the mankind's craving for more and more comfort have resulted in a consistent rise in the demand for electricity. To meet this escalating demand, the number of conventional power generating stations has increased drastically, causing enormous stress on the existing infrastructure. This has led to a rapid depletion of conventional fuel reserves. On the other hand, growing concerns about the harmful effects of conventional fuels on the environment have further complicated the issue and have forced mankind's attention toward renewable energy sources, such as solar photovoltaic (PV), wind, fuel cell stack, biomass, tidal energy, etc., to supplement the growing need of electric energy [1]. Out of these, solar PV and wind have emerged as popular sources as they are both clean and cost effective sources that apparently do not require any fuel [1]–[3] (unlike fuel cell stack, biogas, etc.). Electricity generation from wind energy and its integration with power grid is a well-established technology.

Wind farms with doubly fed induction generators (DFIGs) are time-tested systems for widely varying wind velocity-based variable speed turbine systems [4]. Various control schemes have been developed to enhance the performance of wind-sourced DFIG systems, including those for distorted grid conditions, weak area electric power system, etc. [4]–[8]. Liu *et al*. [7] and Xu *et al*. [8] have discussed elegant solutions for harmonic suppression in stator circuits using rotor-side converter control. Nian and Song [9] have proposed a modified control scheme to smoothen out the

overall active and reactive power output of DFIG under distorted grid voltage conditions. At the same time, in the last couple of decades, solar PV-based power generation has also emerged as a strong option.

It is a pollution free, noise free, and maintenance free source of energy with no additional mechanical or rotating assembly. Significant advancements and refined control strategies have been reported in the recent past for large capacity grid-connected PV systems [10], [11]. These systems are generally either two power stage or single power stage. Most of these configurations employ a grid-side voltage-source inverter (VSI). In the DFIG-based wind energy system, the stator circuit carries the bulk power while the rotor provides the balance power on account of wind speed variation during DFIG's sub- or supersynchronous speed operation. This results in the requirement of lower rating power converters for rotor power conditioning ,which is especially attractive in the Mega-Watt range installations of wind energy systems [6]. Unfortunately, the converters used in the rotor circuit are not utilized effectively because of topological and configuration constraints. During operation near the synchronous speed, rotor power is considerably less.

Another issue with the conventional wind-DFIG system is that part of the power simply circulates in the machine during its subsynchronous operation. In contrast with the DFIG integrated wind energy source, the inverter driven, inertia less PV-grid interfaces result in complex penetration issues such as poor line voltage profile, reduced dynamic stability, voltage fluctuations, and large injected power variations, etc. [12]–[14]. At the same time, the PV inverter remains idle during the night or during very low solar radiation.

Extensive efforts have been made by researchers in the past to overcome the issues associated with both PV and wind energy sources by proposing more advanced and refined control schemes, including their hybrid combinations [2], [3], [15]– [18]. Kellogg *et al*. [2] have investigated the sizing of generators in a hybrid system, in which the sources and storage are interfaced at the dc link, through their individual source converters.

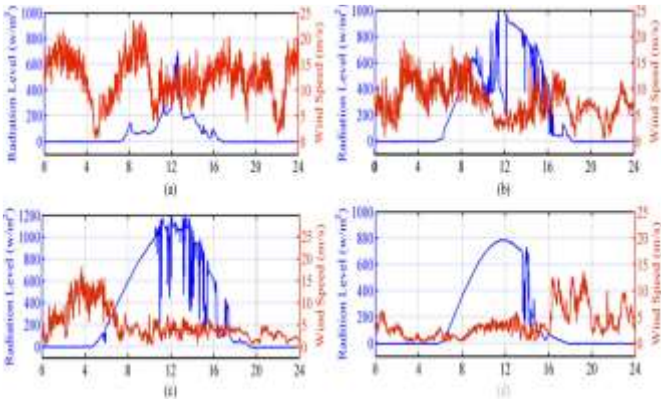

Fig. 1. Solar radiation and wind velocity data (per minute basis) collected from www.nrel.gov for: (a) 01 Jan. 2011, (b) 01 Apr. 2011, (c) 01 July 2011, and (d) 01 Oct. 2011 (Location: latitude—39.91°N,longitude 105.235°W).

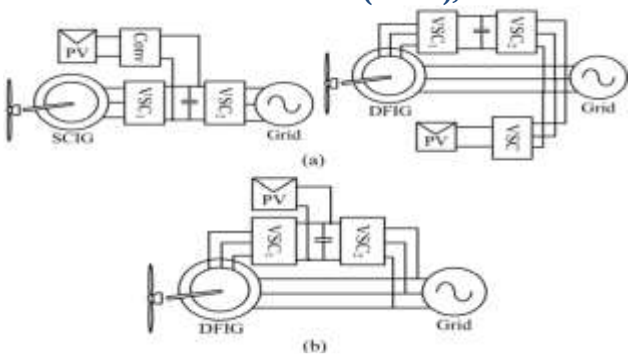

Fig. 2. (a) Block diagram of the conventional PV-wind hybrid systems. (b)Proposed PV-wind hybrid system.

A PV-wind hybrid system, proposed by Daniel and Ammasai Gounden [3], has a simple power topology but is only suitable for stand-alone applications. Chen *et al*. [15] have proposed a multi-input hybrid PV-wind power generation system and focused on improving the dc-link voltage regulation. Here again, the power converters are rated for the individual source power rating. Nejabatkhah *et al*. [18] have proposed a low capacity multi-input port power converter for a hybrid system to feed the dc loads. There is an interesting correlation that exists between the wind and solar energy. The data collected from the NREL [19] website highlight an interesting complementary behavior of solar radiation and wind velocity patterns as shown in Fig. 1.

This fact, coupled with other advantages offered by these two sources, has led the researchers to try and integrate them resulting in what are called the hybrid solar PV-wind systems. Some of the representative hybrid configurations are shown in Fig. 2(a). This paper is focused on a hybrid PV-wind energy generation system that overcomes several drawbacks of the individual PV and wind energy sources described in the preceding paragraphs. An inherent advantage of hybrid solar PV-wind energy system is the reduction in the overall variation in the power output. Unfortunately, not many attempts have been made to optimize the operation and circuit configuration of such systems that could reduce the cost and increase the efficiency and reliability. Further, no research ideas have been reported for large PV integration with power capacity above its dedicated inverter rating. In the existing hybrid systems, both PV and wind sources are associated with their own power converters [2], [15], [17] even though these converters are not properly utilized because of highly intermittent nature of the two sources. Further, many critical issues associated with high power penetration of the inverter coupled hybrid sources in to the grid, such as voltage variation, harmonic injection, circulating power, and dynamic stability need to be investigated in more depth [12]–[14]. Efficiency and cost of the hybrid systems are the other important parameters that have a significant research potential. Another promising topology has been proposed by Qu and Qiao [20], where the dc link of the DFIG is integrated with energy storage (supercapacitor) using a separate dc–dc bidirectional converter to address the intermittent nature of wind energy. Arani and El-Saadany [21] have used a similar system configuration but for incorporating "virtual" inertia to improve system stability. Unfortunately, these papers do not consider prominent features such as efficiency, reduction in circulating power, cost, etc. Rather, they focus on the control and coordination aspects in the presence of multiple DGS. In the backdrop of the previous discussion, this paper proposes a cost-effective, efficient, and compact integration of the solar PV and doubly fed induction generator (PV-DFIG)-based wind turbine system as shown in Fig. 2(b). In the proposed scheme, the grid- and rotor-side power converters associated with DFIG are also used to inject PV generated power into the grid. Thus, the proposed configuration and control scheme provide an elegant and economical integration of PV source and DFIG-based wind energy source.

The proposed hybrid system offers the following advantages:
1) Enhanced power conversion efficiency is realized as a dedicated inverter for the PV source is no longer required. PV installation utilizes rotor circuit converters (VSC1 and VSC2) of the DFIG.
2) Reduction in the overall cost of the system, as one VSI and its associated control circuit (including DSP controller) are eliminated from the conventional hybrid system.

3) It facilitates the possible interfacing of a higher rating PV source compared to the dedicated inverter in the conventional interface.
4) It results in increased and optimal utilization of power converters.
5) It reduces the circulating power flow in the DFIG system during low speed operation and high solar radiation. This cuts down the losses of the overall system.
6) Maximum power point tracking (MPPT) of the PV installation is realized in conjunction with the dc bus voltage control to extract optimum power from the PV source. The wind turbine system is controlled with the maximum power extraction algorithm in conjunction with pitch control to avoid overloading in case of high wind velocity.
7) Variation in the grid-injected power over a day is minimized. Idle condition of PV VSI is nearly eliminated. A bare minimum power delivery from the hybrid system is maintained throughout the day and across the seasons.
This is not true for systems fed either by solar PV or wind turbine sources alone.
8) The proposed hybrid system has scope for integration of energy storage for enhancing power quality and reliability in terms of continuity and availability of the power supply. The overall power injection from this hybrid system to the grid is averaged by the intermittent but complementary sources of PV and wind.
9) A modified PV power control algorithm incorporated in the control scheme can tackle any of the environmental conditions in case of both high radiation and wind velocity level occurring simultaneously.

DESCRIPTION OF THE PROPOSED SYSTEM

This section describes the proposed integration of the solar PV and wind-sourced DFIG system and presents its modelling and control aspects.

A. System Description

The schematic of the proposed system is shown in Fig. 3. A wind DFIG system of 1MWcapacity is considered in this study along with a PV generation of comparable rating. The stator circuit of the DFIG is coupled to the grid through the circuit breaker, *S*2 . Normally, rotor circuit converters (both grid and rotor sides) with 25% rated system capacity are sufficient for handling a part of the total turbine generated power over the operating range based on maximum allowable slip [22].

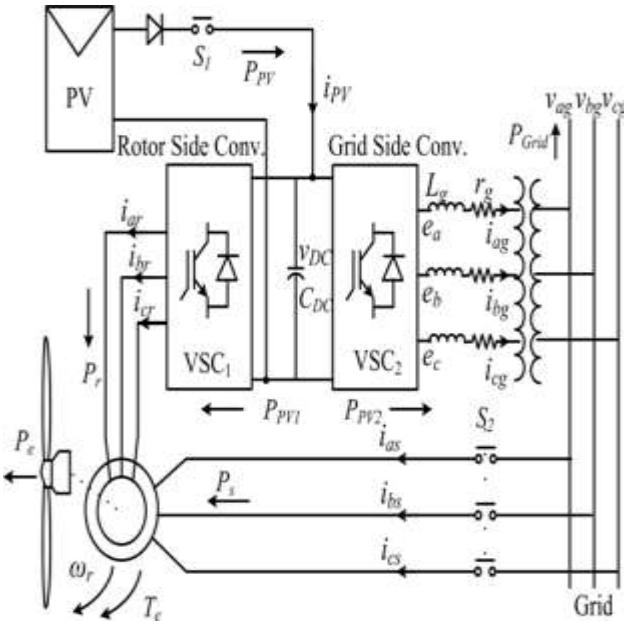

Fig. 3. Proposed solar PV-wind DFIG system

In this study, the rotor-side converter (VSC1) is rated for 250 kVA, while the grid-side converter is rated at 340 kVA. To highlight a major advantage of the proposed hybrid system, a 380 kW capacity PV source is considered which is

significantly higher than the grid-side converter rating (VSC2). Later, it is demonstrated that a PV source with much larger rating, compared to the inverter capacity used in a conventional grid-tied PV system, can be integrated with the wind-DFIG system without an additional dedicated inverter. Though the rotor-side converter (VSC1) can support system operation over a wide speed range, pitch control is provided to ensure optimal energy extraction and protection against excessive wind turbulence and overloading. The PV source is protected with an antiblocking diode and dc circuit breaker *S*1 whose operation is integrated into the overall control strategy. In addition to this, a modified algorithm is incorporated to control the PV power using dc-bus voltage control (rather than only MPPT control). This protects VSC2 from overloading. Both rotor- and grid-side control are crucial for the successful operation of the proposed system. Fig. 3 also shows the parameter descriptions of the proposed system, which have been considered for modeling and controller design.

B. System Modeling of DFIG

Vector control is a powerful tool for controlling the desired parameters of a $3-\phi$ system. A reference frame transformation technique is used with *d*-axis of the frame aligned with the space vector of stator flux that rotates at a synchronous speed, ωo [22], [23]. The stator and rotor equations in *d–q* reference frame in transformed vector form (*fdq = fd + jfq*) are given as next and used to derive the dependence of rotor power on rotor speed

$$v_{dqs} = r_s i_{dqs} + \frac{d}{dt}\psi_{dqs} + j\omega_o \psi_{dqs} \qquad (1)$$

$$v_{dqr} = r_r i_{dqr} + \frac{d}{dt}\psi_{dqr} + j(\omega_o - \omega_r)\psi_{dqr} \qquad (2)$$

where *vdqs* is the transformed stator voltage vector (and is equal to the grid voltage vector), *vdqr* is the rotor terminal voltagevector (after averaging, to exclude higher order switching components), which is controlled by VSC1 ; *idqs* and *idqr* are the stator and rotor current vectors and ωr is the rotor speed in rad/s. ψdqs and ψdqr are the stator and rotor flux vectors, related with stator, rotor currents and magnetizing inductances, *Ls* , *Lr* ,
and *Lm*, respectively, as follows:

$$\psi_{dqs} = L_s i_{dqs} + L_m i_{dqr} \qquad (3)$$

$$\psi_{dqr} = L_m i_{dqs} + L_r i_{dqr}. \qquad (4)$$

ψds is the *d*-axis component of the stator flux (ψdqs) and in this case is equal to the stator flux vector amplitude. Thus, for stator voltage amplitude (*Vms*), $\psi ds = |\psi dqs| = Vms/\omega o$, assuming the stator resistance drop to be very small compared to stator terminal voltages and $\psi qs = 0$. The reference frame transformation technique facilitates independent control of the stator's active and reactive power by *d–q* components of the rotor current. Further, these components are dc values under steady state and hence they are easy to control with traditional PI-PID controllers with a sufficiently large bandwidth and minimum steady-state error. In (2), replacing the rotor flux vector by (4), and further replacing all stator current components with rotor current components using (3), the following machine model can be derived in terms of rotor current components [24]:

$$\sigma L_r \frac{di_{dr}}{dt} = -r_r i_{dr} + \omega\sigma L_r i_{qr} + v_{dr} - \frac{L_m}{L_s}\frac{d}{dt}\psi_{ds}$$

$$\sigma L_r \frac{di_{qr}}{dt} = -r_r i_{qr} - \omega\sigma L_r i_{dr} + v_{qr} - \omega\frac{L_m}{L_s}\psi_{ds} \qquad (5)$$

where leakage coefficient, $\sigma = 1 - L^2_m/L_sL_r$; angular frequency of transformation for the rotor-side quantities is $\omega = d\theta/dt$ and θ is obtained from flux estimator.Alternatively, using phaselocked loop (PLL) with the grid supply voltage and rotor position θ_r (from position encoder), an approximate flux vector location in quadrature with the grid voltage vector can be determined [25]. In steady state, frequency of the rotor current is equal to the slip frequency, $\omega = \omega_o - \omega_r$. The electromagnetic torque *Te* generated by the machine can be determined from vector product of rotor flux and rotor current as follows:

$$T_e = p\frac{3}{2}\frac{L_m}{L_s}\mathrm{Img}\left(\psi_{dqs} i^*_{dqr}\right) = -p\frac{3}{2}\frac{L_m}{L_s}\frac{V_{ms}}{\omega_o} i_{qr} \qquad (6)$$

where p is the number of pole pairs. Using (6), the electromagnetic power P_e generated at rotor speed ω_r is given by

$$P_e = -\frac{3}{2}\frac{L_m}{L_s}\frac{\omega_r}{\omega_o} V_{ms} i_{qr}. \qquad (7)$$

Thus, throughout the generation mode, the component i_{qr} remains positive and can independently control P_e Similarly, the stator power P_s can determined from $Ps = 3/2 v_{qs} i_{qs}$ with the assumption that stator drop is very small and voltage vector is in quadrature with the flux vector. Thus

$$P_s = -\frac{3}{2}\frac{L_m}{L_s} V_{ms} i_{qr} \qquad (8)$$

Where $i_{qs} = -(L_m/L_s) i_{qr}$

The rotor power P_r can be determined as follows:

$$P_r = \frac{3}{2}\frac{L_m}{L_s}\frac{(\omega_o - \omega_r)}{\omega_o} V_{ms} i_{qr}. \qquad (9)$$

From (9), a very important inference can be made that, during subsynchronous operation (which happens during low wind velocities) in the generation mode, the direction of rotor power is from VSC_1 toward the rotor terminals.

C. DFIG Control

DFIG rotor current model (5) is nonlinear in nature and is coupled with both rotor current parameters, i_{dr} and i_{qr}. The rotor terminal voltages v_{dr} and v_{qr} are controlled by VSC1 through modulation indices m_{dr} and m_{qr} . A sinusoidal pulse width modulation (PWM) technique is used for both VSC1 and VSC2 . Decoupling and feed-forward compensation are invoked to independently control the rotor circuit current components by using the following decoupled model:

$$\begin{aligned} \sigma L_r \frac{di_{dr}}{dt} &= -r_r i_{dr} + n_1 \\ \sigma L_r \frac{di_{qr}}{dt} &= -r_r i_{qr} + n_2 \end{aligned} \qquad (10)$$

where n_1 and n_2 are the new control variables related with original control parameters m_{dr} and m_{qr} as follows:

$$\begin{aligned} m_{dr} &= \frac{2}{v_{\mathrm{DC}}}(n_1 - \omega\sigma L_r i_{qr}) \\ m_{qr} &= \frac{2}{v_{\mathrm{DC}}}\left(n_2 + \omega\sigma L_r i_{dr} + \frac{\omega}{\omega_o}\frac{L_m}{L_s} V_{ms}\right). \end{aligned} \qquad (11)$$

The dc-link voltage v_{DC} is considered to be constant during the current control operation as it is supported by a large capacitor bank and also controlled by VSC_2 with relatively less bandwidth of the dc-link voltage control. During the entire operation, the stator flux is tightly held by grid supply voltage, and its magnitude remains constant except during starting (for machine excitation). Hence, its time derivative is considered to
be zero. Using (10), the transfer function G_{ir} can be derived for the control of rotor current components. Both i_{dr} and i_{qr} have the same plant transfer function as follows:

$$G_{ir} = \frac{I_{dr}(s)}{N_1(s)} = \frac{I_{qr}(s)}{N_2(s)} = \frac{1}{\sigma L_r s + r_r}. \qquad (12)$$

PI controller, G_{Cir} is a suitable choice for the first-order plant transfer function (12), with PI zero cancelling out the dominant pole located at $s = -r_r / \sigma L_r$. This results in a first-order transfer function of the closed-loop current control system with time constant T_{cr} and is designed to achieve desired bandwidth (1/10th of the switching frequency of VSC1 appr). With this understanding and using (12), the PI compensator parameters are given by

$$K_{Pr} = \frac{\sigma L_r}{T_{cr}}; \quad K_{ir} = \frac{r_r}{T_{cr}}. \qquad (13)$$

The wind turbine-driven DFIG can be controlled over a considerable speed range to achieve maximum power yield $Ps|_{\max}$

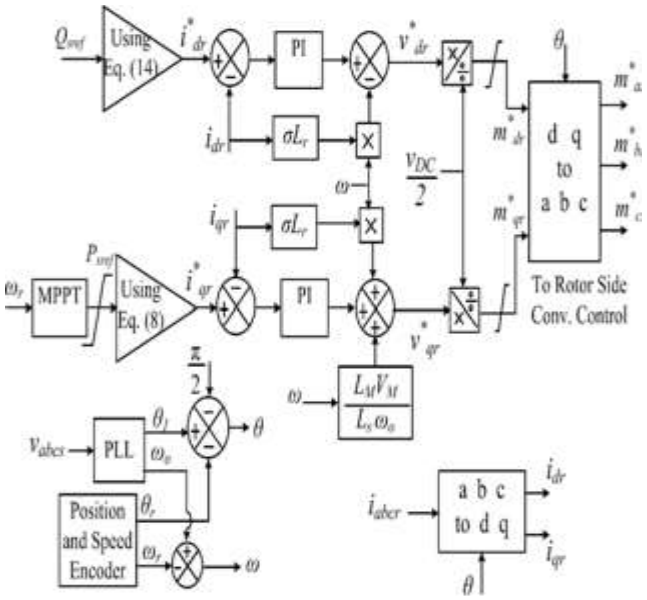

Fig. 4. Rotor-side converter, VSC₁ control.

without exceeding the turbine's rated power capacity. Any conventional MPPT algorithm can be employed to track the wind turbine's peak power which is a function of the wind velocity v_W and turbine speed ω_r [26], [27]. As a supplementary functionality, DFIG can be controlled to improve line voltage profile or for reactive power support. The stator reactive power is related to i_{dr} and can be independently controlled for unity p.f. operation or for the reactive power compensation [22] as per the following relation:

$$Q_s = \frac{3}{2}\frac{V_m^2}{\omega_o L_s} - \frac{3}{2}\frac{L_m V_m^2}{L_s} i_{dr}. \qquad (14)$$

In order to minimize loading of VSC1 and to avoid large current to flow, reference i^*_{dr} can be set to zero.
The control strategy for the rotor-side converter (see Fig. 4) is based on (8), (11), and (13) and involves the control of rotor current.

D.* VSC₂ *and PV Power Control

Starting with space vector equation in synchronously rotating reference frame, the grid-side converter (VSC_2) current model, after segregating the components into real and imaginary parts, is represented by [24]

$$L_g \frac{di_{dg}}{dt} = -r_g i_{dg} + L_g \omega_o i_{qg} + \frac{V_{DC}}{2} m_{dg} - v_{dg}$$
$$L_g \frac{di_{qg}}{dt} = -r_g i_{qg} - L_g \omega_o i_{dg} + \frac{V_{DC}}{2} m_{qg} - v_{qg} \qquad (15)$$

where v_{dg} and v_{qg} are the components of the transformed grid voltages (which have same space vector as that of stator terminal voltages). In this case, *d*-axis of reference frame is aligned with the voltage vector, i.e., $v_{qs} = 0$ and i_{dg} and i_{qg} are the current components.
New variables y_{dg} and y_{qg} can be introduced in (15) to obtain the transfer function, G_{ig} to enable the design of the inner current loops as follows:

$$G_{ig} = \frac{I_{dg}(s)}{Y_{dg}(s)} = \frac{I_{qg}(s)}{Y_{qg}(s)} = \frac{1}{L_g s + r_g}. \qquad (16)$$

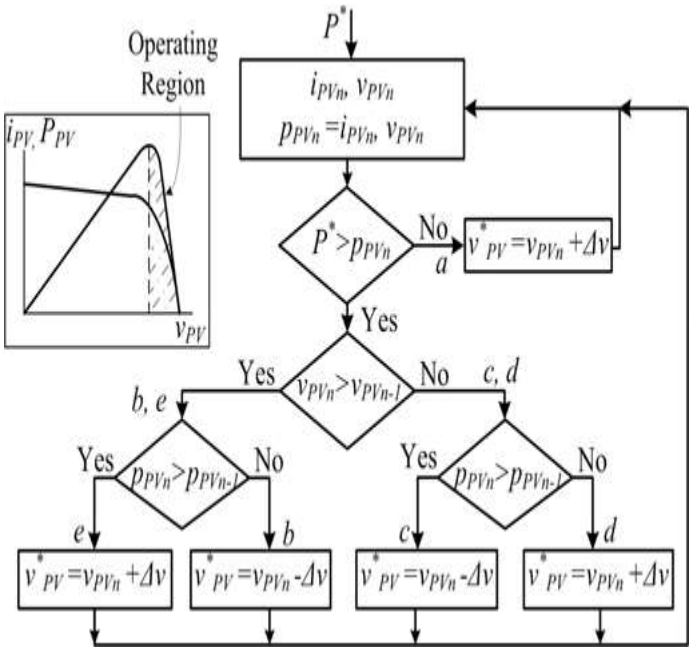

Fig. 5. PV power control algorithm for the proposed hybrid PV-wind system.

The modulation indices m_{dg} and m_{qg} can be determined as follows to incorporate decoupling and feed-forward compensation:

$$m_{dg} = \frac{2}{V_{DC}} (y_{dg} - L_g \omega_o i_{qg} + v_{dg})$$
$$m_{qg} = \frac{2}{V_{DC}} (y_{qg} + L_g \omega_o i_{dg}). \qquad (17)$$

Similar approach that is used to design G_{Cir} is used to design the PI compensator, G_{Cig} for the inner current control loop of VSC_2 . Thus, elements of G_{Cig} are

$$K_{Pig} = \frac{L_g}{T_{cig}};\ K_{Iig} = \frac{r_g}{T_{cig}} \qquad (18)$$

Where K_{Pig} and $K_{I\,ig}$ are the PI controller's proportional and integral parameters, respectively.
With the previous compensator parameters, the closed-loop transfer function of the current control loop G_{CL} can be reduced to first order with unity gain as follows:

$$G_{\mathrm{CL}}(s) = \frac{1}{T_{cig}s + 1}. \qquad (19)$$

v_{DC} was assumed to be a constant for the design of inner current control. In the proposed scheme, PV power is controlled by regulating v_{DC} and ensuring that the operation does not shift to the over modulation range. Fig. 5 shows the proposed modified algorithm for the control of PV power. This algorithm incorporates MPPT (like conventional methods) for optimum power and also precise power control (unlike conventional methods) depending upon the operating mode (DFIG sub- or supersynchronous speed), environmental conditions, and VSC_2 loading. Plant model for the PV terminal (dc link) voltage control can be determined from the power balance condition across the dc and ac ports of VSC_2 as follows:

$$P_{\mathrm{PV}} = \frac{d}{dt}\frac{1}{2}C_{\mathrm{DC}}v_{\mathrm{DC}}^2 + P_r + \frac{3}{2}v_{dg}i_{dg}. \qquad (20)$$

Assuming the inner current control loop of VSC2 to be considerably faster (T_{cig} is small), the reference, i^*_{dg} is used as the controlling parameter for dc-bus voltage regulation. v^2_{DC} is a state as well as an output variable while i^*_{dg} is the control variable and input to the inner current control loop. Using a new variable p_h , the transfer function G_V can be written as follows:

$$G_V(s) = \frac{V_{\mathrm{DC}}^2(s)}{P_h(s)} = \frac{2}{C_{\mathrm{DC}}s} \qquad (21)$$

where i^*_{dg} is related to p_h as follows:

$$i_{dg}^* = \frac{2}{3V_{mg}}(-p_h + P_{\mathrm{PV}} - P_r). \qquad (22)$$

Rotor power P_r [using (9)] and PV power P_{PV} from measurement may be provided for feed-forward compensation to improve dynamic response against disturbances. The loss component of the converter and that of dc-link cannot be measured. Therefore, the integral term is added with a lead compensator to achieve zero steady-state error and sufficient phase margin. A phase boost (φ_{boost}) at the required cut-off frequency
(ω_{CV}) of the gain plot can be designed such that $\omega_{\mathrm{CV}} \approx 0.1$ to $0.3 \times 1/T_{cig}$. Thus, G_{CV} has the following form:

$$G_{\mathrm{CV}}(s) = \frac{h}{s}\frac{s + r/\alpha}{s + r} \qquad (23)$$

where

$$r = \omega_{\mathrm{CV}}\sqrt{\alpha},\ \alpha = \frac{1 + \sin\phi_{\mathrm{Boost}}}{1 - \sin\phi_{\mathrm{Boost}}}$$

and h is adjusted such that the gain plot cuts the frequency axis at ω_{CV}.
The control scheme proposed in this paper, for the grid-side converter, differs from the conventional control schemes in the following respect:

1) in the proposed system, the control scheme presented for grid-side converter has been incorporated with a special (modified) PV power control algorithm and not just a conventional MPPT control;
2) an additional control loop has been incorporated in the proposed system to tackle the "worst case" environmental impact (i.e., high solar radiation and high wind velocity existing at the same time) by automatically adjusting VSC_2 loading;
3) during most of the time, the PV and the wind systems operate at MPP. However, during a harsh sunny day and heavy wind conditions occurring simultaneously, the PV operating point shifts fromMPPso as to avoid overloading of VSC_2 .

VSC_2 control strategy is shown in Fig. 6, which includes grid-side inner current control and outer dc-link (PV terminal) voltage control. It also incorporates the PV power control algorithm shown in Fig. 5 to ensure optimum utilization of both converters. The reference power generation block (A) provides the value of $P*$ to the PV power control algorithm which, in turn, provides the reference dc-link voltage (V * dc) to the active power loop (B) in Fig. 6. During most of the day time operation, reference $P*$ remains higher than the maximum power available with PV panels. Table I shows the parameters of the hybrid system under study and final form of controllers determined from the previous procedure. The parameters given in Table I are used to determine the controller elements. Dynamic behavior of various control loops can be examined from the Bode plots for both the VSCs as shown in Fig. 7.

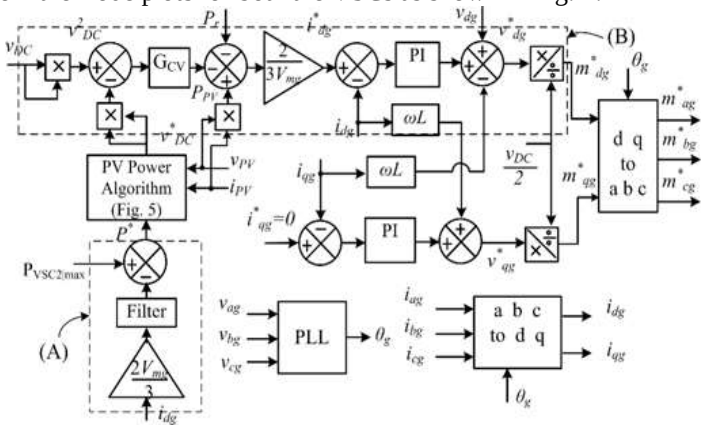

Fig. 6. Proposed control strategy for the grid-side inverter, VSC_2

TABLE I CONTROL DESIGN PARAMETERS

Element	Parameter	Element	Parameter
Turbine nominal power	1 MW	Magnetizing Inductance L_m	30 mH
Nominal voltage	690 V	Pole pairs	2
Nominal frequency	50 Hz	Stator resistance R_s	40 mΩ
Turbine speed range	900–1800 r/min	Rotor resistance R_r	32 mΩ
Switch freq. of VSC_1 and VSC_2	7 kHz	VSC_2 filter (L_g and R_g)	200 μH, 15 mΩ
PV capacity	380 kW	Transformer ratio N1:N2	1:2
V_{MP} at 1000 W/m²	640 V	VSC_1 current controller	$G_{CIr}(s) = \frac{5.32s+140}{s}$
V_{DC} range	580–710 V	VSC_2 current controller	$G_{CIg}(s) = \frac{0.88s+65}{s}$
VSC_1 capacity	250 kVA	DC-bus voltage controller	$G_{CV}(s) = \frac{7255}{s}\left(\frac{s+118}{s+1640}\right)$
VSC_2 capacity	340 kVA	Perturbation ΔV	0.5 V
Stator inductance L_s	30.6 mH	Algorithm update rate	30 ms
Rotor inductance L_r	30.6 mH	–	–

POWER CONVERSION ANALYSIS OF THE PROPOSED SYSTEM

In this section, power conversion analysis is presented to highlight the relation between *PP V* and *PV SC*2 and to conclude about their ratings. Fig. 8 shows the power conversion process in various stages of the proposed hybrid system (during most of the day time), shown as per actual power flow direction. Complementary nature of solar radiation and wind enables the interfacing of a large PV installation in the proposed system with a capacity significantly higher than the grid-side converter (VSC_2) rating. From (7) and (9)

$$P_r = \frac{\omega_r - \omega_o}{\omega_r} P_e. \qquad (24)$$

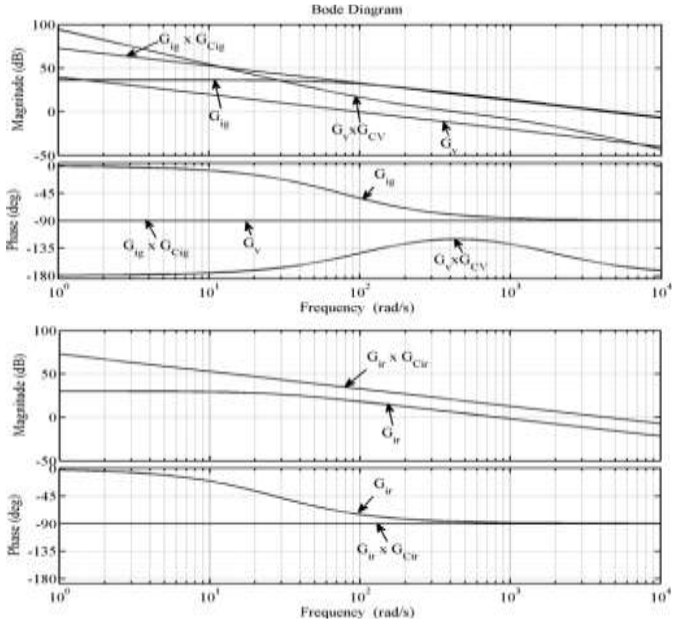

Fig. 7. Bode plots for the designed compensators ofVSC_2 andVSC_1 control

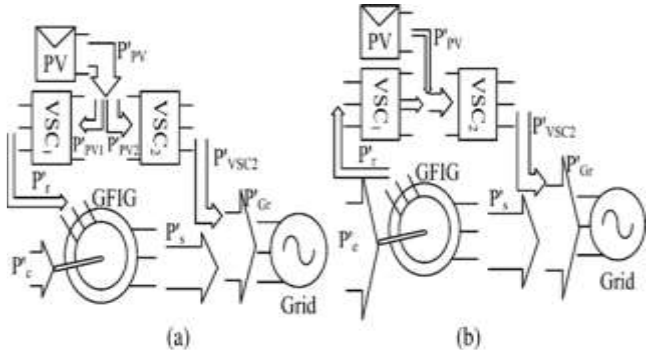

Fig. 8. Power conversion process in various segments of the proposed hybrid PV-wind-energy system during most of the day (as per actual power flow direction indicated by P^1_r P^1_{SC2} , etc.).

(a) High solar radiation, low wind speed. (b) Low solar radiation (or during nights), high wind speed.

Following the circuit conventions of Fig. 2, one can write

$$P_{VSC2} = P_{PV} - P_r. \qquad (25)$$

From (7)–(9), it is clear that the steady-state power balance equation of a DFIG is a function of rotor speed "ω_r ." During the day time, wind velocity is generally low and solar radiation level is high. Under these conditions, the wind

turbine system is controlled with MPPT and operates below the synchronous speed "ω_o" Hence, during the generating mode of operation, i.e., P_e is −ve, which results in the following power flow in the various stages:
1) P_r becomes +ve: machine receives power through the rotor circuit as per (24), it is proportional to the slip speed;
2) P_s becomes −ve: machine delivers power through stator to the grid as per (7) and (8);
3) P_{PV} is +ve: the solar PV generated power splits into two components, one goes toward rotor circuit and the other toward the grid-side converter;
4) P_{VSC2} is +ve: it is the differential power flow through VSC_2 as per (25). The PV generated power can be bifurcated into two parts for the purpose of understanding as follows:

$$P_{\mathrm{PV}} = P_{\mathrm{PV1}} + P_{\mathrm{PV2}} \qquad (26)$$

where the component P_{PV1} is directed to the rotor circuit of the machine through VSC_1 during the subsynchronous operation and may be considered as compensation power of the rotor circuit. The P_{PV2} component corresponds to the bulk surplus power injected into the grid through VSC2 . In this case, power flow is represented by

$$P_{\mathrm{PV1}} = P_r \qquad (27)$$

$$|P_s| = |P_e| + |P_{\mathrm{PV1}}| \qquad (28)$$

$$P_{\mathrm{VSC2}} = P_{\mathrm{PV2}}. \qquad (29)$$

Turbine power versus speed (P_e versus ω_r) characteristic of the DFIG wind system consists of the constant low speed region, the maximum power extraction region, and the constant nominal speed region. During the low wind velocity, turbine operates in between the region of constant low turbine speed up to the synchronous speed of the maximum power extraction region. Referring to Fig. 8(a) and from (28) and (29), it is clear that the solar PV power is injected into the grid via two paths.During this region, the machine receives power through VSC_1 as per (24) and it is finite. Also, as $P_{PV\ 1} = P_{VSC1}$, the following relation can bededuced:

$$P_{\mathrm{VSC2}} < P_{\mathrm{PV}}. \qquad (30)$$

From (30), it may be concluded that the PV capacity can be more than VSC_2 rating. This is graphically depicted in Fig. 8(a). In other words, if VSC_2 is considered as the PV inverter of the conventional PV-grid system, then with the proposed hybrid integration, the installed PV capacity can be increased beyond the inverter rating. In the conventional grid tied system, the VSC regulates the dc-link voltage by incorporating power balance between the ac and dc ports (of the VSC). However, in the proposed hybrid system configuration, the PV power not only compensates the dc-link losses to regulate its voltage indirectly through VSC_2 , but also the PV power is bifurcated into two parts depending upon the mode of operation, unlike a conventional DFIG system. One part of the PV power flows through the rotor circuit (VSC_1) and the other part is injected into the grid through VSC2 . This provides an opportunity to install a PV source with power capacity more than the VSC_2 kVA rating. This is not the case with existing hybrid solutions. The proposed configuration drastically reduces the circulating power that is common in conventional DFIG systems and hence enhances the overall efficiency. During low radiation and high wind velocity phase, the turbine operates at supersynchronous speed (i.e., P_r is −ve) and the PV power is not significant to overload VSC_2 even though rotor power Pr is also routed through VSC2 . This condition is depicted in Fig. 8(b). Though rare, both wind and solar radiation may be high simultaneously. During this condition, control scheme of Fig. 6 is capable of optimally utilizing VSC2 by reducing the PV power generation. The proposed hybrid system also provides scope for incorporating energy storage for further enhancing the power quality and reliability to improve the continuity and availability of the power supply.

SIMULATION VERIFICATION

Dynamic performance of the complete control scheme for various stages of the proposed hybrid PV/DFIG system is evaluated in this section. The complete system described in Section II is modeled in MATLAB-Simulink software for validation of the proposed PV-wind hybrid system. The parameters listed in Table I are used for the simulations. To

evaluate the important aspects of the proposed system, wind velocity and hence turbine speed are varied in the regions of subsynchronous and supersynchronous speed as shown in

Fig. 9(a) by keeping turbine-machine combined inertia very low and directly controlling the speed parameter of the inbuilt MATLABmodel. Similarly, solar radiation is also varied so as to cover most frequently occurring events (including worst events) as shown in the same figure. Solar PV breaker, *S*1 is excited at time t = 1 s with radiation 1000 W/m2 and later changed to 500 W/m2 at t = 3.5 s and 700 W/m2 at t = 4.7 s, respectively. The proposed PV power control algorithm described in Section II determines the dc-link voltage as per the situation and controls it using VSC2 dc-link voltage controller as shown in Fig. 9(b). Before exciting the PV-side breaker (*S*1), dc link is regulated at a nominal value of 670 V. A rotor-side converter is activated at time t = 0.5 s. When machine is operating in subsynchronous mode, the PV power is routed through both rotor-side and grid-side converters. Hence, in spite of large power flow, the PV source still operates at MPP (controlled by the algorithm in Fig. 5) and adjusts the dc-link voltage at *vMP* as shown in Fig. 9(b) during time intervals t = 1–3 s and t = 3.5–5 s. However, during supersynchronous operation, the PV algorithm controls the flow of PV power so as to prevent the overloading of VSC2 by controlling dc-link voltage and hence PV terminal voltage. This may be seen during the interval t = 3–3.5 s. Fig. 9(c) shows the behavior of rotor current with respect to slip speed and is responsible for the extraction of maximum turbine power using stator power control. The rotor active power *PRt* and reactive power *QRt* are shown in Fig. 9(d). It brings out a very important observation that during low wind speed (i.e., $\omega r < \omega o$), the rotor power is positive and flowing into the rotor circuit through VSC1 . During the day time when the solar radiation is high, part of PV power is shared by *PRt* and only remaining PV power is fed by VSC2. The reactive power support is to achieve unity p.f. operation on the stator side. Fig. 9(e) shows the stator active and reactive power components. The current feedback of VSC2 is also used to determine the PV power reference $P*$ (see Figs. 5 and 6). During normal operation, VSC2 controls the PV terminal voltage at MPP as shown in Fig. 9(f). But during high wind velocity and high radiation occurring simultaneously, the algorithm (see Fig. 5) limits the VSC2 power at its maximum rated capacity as can be seen during time interval t = 3–3.5 s. Small oscillations are observed during this interval as point of operation lies on the stiff slope of PV power. Fig. 9(g) shows the PV generated power. The complete system injects considerable amount of power into the grid from both wind and PV sources as shown in Fig. 9(h). Clearly, the total PV-wind hybrid system power is enhanced due to the contribution of the PV power. Analytically derived controllers in Section II show satisfactory tracking performance as revealed from Fig. 9(b), (i), and (j) for dc-link voltage, VSC2 and VSC1 currents, respectively. Steady-state performance of the proposed hybrid system over a day has been evaluated using the wind and solar radiation data [see Fig. 1(b)]. Power balance equations have been used to determine power flowduring various stages corresponding to the per minute data of solar radiation and wind velocity. MPPT has been assumed for both PV and wind sources unless the power flow through VSC2 reaches its rated capacity. Fig. 10(a) shows the power flow in various sections, e.g., rotor power *Pr* (the same as power through VSC1), VSC2 power, turbine generated power *Pe* , and PV power *PP V* . It is observed from the plot that during most of the day time both PV and wind turbine operate in MPPT mode. Their complementary nature helps to achieve optimum power yield from both the sources without overloading any of the converters in the proposed system. It is also observed that for a short time around 9.00 A.M., the PV power can be controlled using the proposed algorithm so as to avoid the overloading of VSC2 . The same data are used to determine the loading of VSC2 over the day and results are plotted in Fig. 10(b) for every minute. It is observed that the operational cloud is dense during light loading. Further, there are very few operating points, which need to be clamped at the rated capacity of VSC2 to avoid its overloading. This results in an overall reduction in power loss because of the PV control algorithm. The efficiency performance of the proposed PV/wind system is evaluated using the data provided in Fig. 1(b) and compared with the conventional distributed PV and wind sources (with DFIG) of similar capacity. Typical plots of the conversion efficiency of the converters and machine with respect to their loading have been used for the analysis and comparison of the two cases: 1) conventional PV-inverter and wind-DFIG system where sources are associated with their individual power converters; and 2) proposed hybrid system of PV/wind sources (see Fig. 2). The results are shown in Fig. 10(c).

It is observed that during the day light time the power conversion efficiency of the proposed hybrid system is substantially higher compared to the conventional distributed generation.

ISSN: 2277-9655
(I2OR), Publication Impact Factor: 3.785

EXPERIMENTAL VERIFICATION

A laboratory prototype of the proposed PV-wind hybrid system is developed to evaluate the important aspects of the system. Fig. 11 shows a 2.5 kW DFIG machine with back-to-back

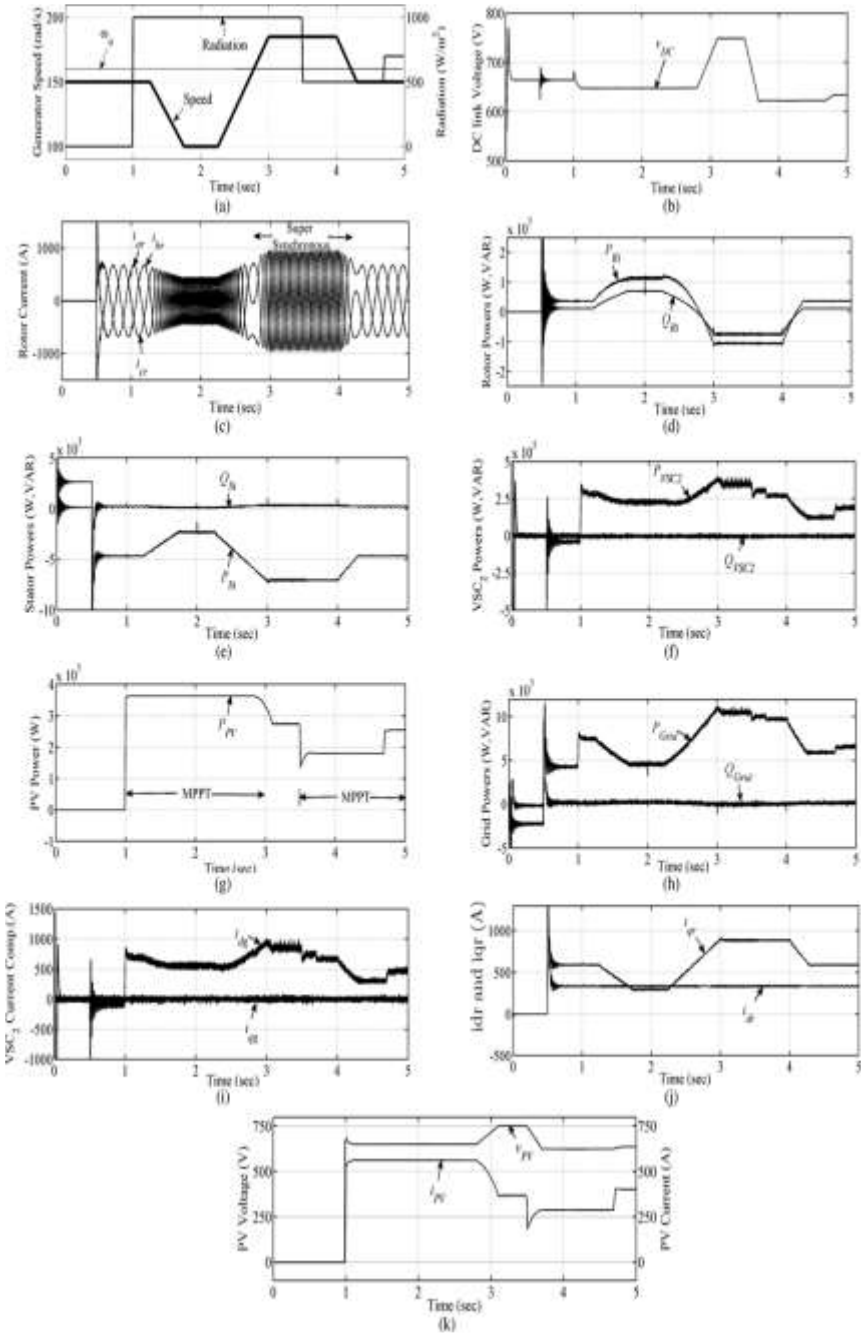

Fig. 9. Simulation results for: (a) machine mechanical speed and radiation pattern applied to the hybrid system; (b) dc-link voltage controlled by the algorithm (see Fig. 5) via VSC_2 ; (c) rotor current performance under different machine speeds; (d), (e) active and reactive components of rotor and stator power; (f) loading of VSC_2 ; (g) PV power generation; (h) power injected into the grid; (i) VSC_2 current components; (j) rotor current components; (k) PV terminal voltage and current

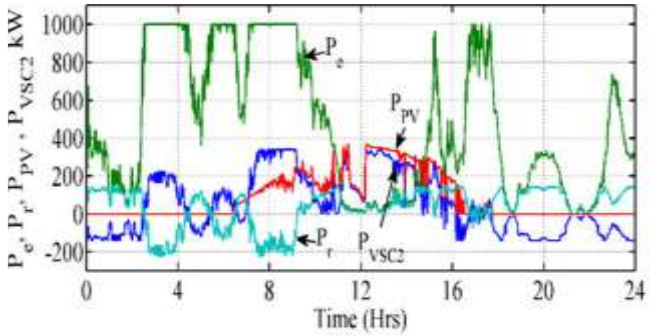

(a)

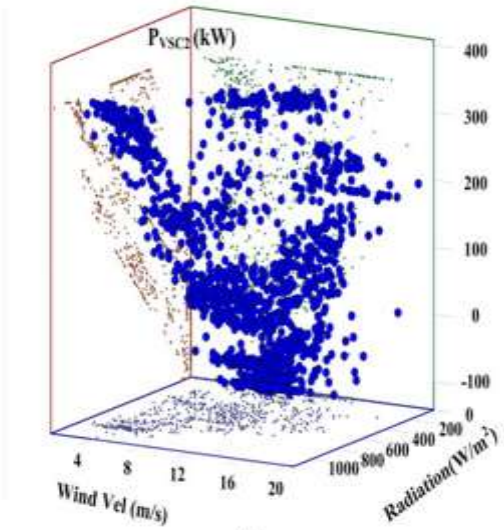

(b)

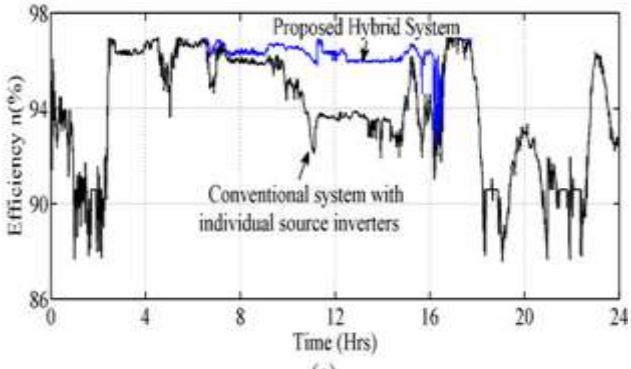

(c)

Fig. 10. Simulation results with per minute data provided in Fig. 1(b) over a day for: (a) power flow in various sections (P_e , P_r , P_{VSC2}, and P_{PV}); (b) VSC_2 loading in kilowatt; (c) efficiency analysis to compare the benefits of the proposed hybrid system with conventional distributed generation having individual source converters.

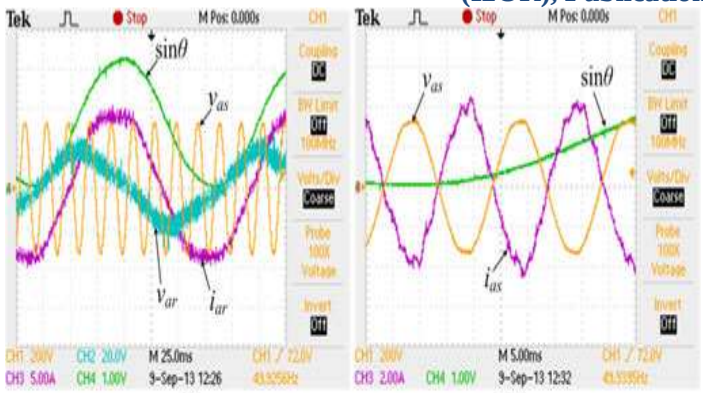

Fig. 11. Experimental results: (a) subsynchronous operating mode showing A-ph rotor current and voltage, A-phase stator voltage, and sine transformation angle for rotor quantities; (b) subsynchronous mode showingA-ph stator voltage and current and sine transformation angle; (c) supersynchronous mode showing the same parameters as in (a).

converters connected to its rotor circuit. TMS320F28035 controller is used. It acquires the required feedback signals, e.g., dc-link voltage, stator voltages, rotor currents, PV current, etc., using signal conditioning circuit via analog channels. Internal PWM modules of the controller are used to drive the back-toback converters through isolated driver circuits. I/O pins are used for the operation of power contactor through an electromagnetic relay. Encoder pulses provide information about the position and speed through a quadrature module. The complete control strategy (see Figs. 4, 5, and 6) is discretized and coded into the TMS320F28035 controller. For the convenience of experimentation and to clearly show the power flow in various sections of the system, the rotor current, i_{qr} is controlled to operate the system in constant stator power mode as per (8) irrespective of the rotor speed, unlike conventional MPPT control of the DFIG. The dc motor driving the DFIG is controlled to cover the operation from subto supersynchronous speed. Fig. 11(a) shows the steady-state waveforms during subsynchronous operation for the A-phase rotor current and voltage in synchronization with "sinθ," where θ is the transformation angle obtained using the position encoder and PLL on grid voltages. This is displayed using a DAC (with the help of PWM pin of the controller and the *R*–*C* filter). The results show that the rotor power is +ve and reactive power is controlled to achieve unity p.f. at stator. The stator power injected in to the grid can be seen in Fig. 11(b), which also shows unity p.f. operation. The rotor speed is later changed to above synchronous speed and the corresponding results are shown in Fig. 12(c), which indicate reversal of rotor power flow direction. However, the stator parameters' waveforms maintain the same trend as before.

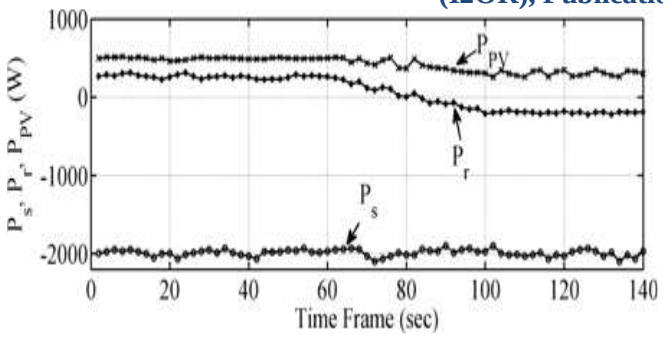

Fig. 12. Experimental results showing stator power, rotor power, and PV power over the complete operating range.

Fig. 12 shows the experimental results for power flow in various sections of the system, captured using a PM6000 power analyzer. These waveforms cover the operating range from subto supersynchronous mode. It may be observed from the figure that, during subsynchronous operation, the rotor power is positive and is responsible for diverting part of the PV power (and hence relieving the grid-side converter, up to some extent). This enables the PV to operate at MPP. It is also observed that the proposed PV power control algorithm works satisfactorily over the complete range ensuring that the solar PV operates in power control mode during supersynchronous speed to avoid overloading of VSC_2

.

CONCLUSION

Nature has provided ample opportunities to mankind to make best use of its resources and still maintain its beauty. In this context, the proposed hybrid PV-wind system provides an elegant integration of the wind turbine and solar PV to extract optimum energy from the two sources. It yields a compact converter system, while incurring reduced cost. The PV generated power can be routed to the grid using both the rotor and grid-side converters of the wind-DFIG system, during its subsynchronous operation. It has been verified that unlike the conventional wind-DFIG system, the circulating power is significantly reduced with PV-DFIG integration at the dc link.

Enhanced efficiency is observed compared to existing PV/wind hybrid systems. It is demonstrated that the proposed hybrid system provides an opportunity to integrate a higher capacity PV source than can be done through a dedicated converter as in a conventional solar PV system. Simulations and experimental results have shown that the proposed system optimally uses the daily available energy from solar and wind sources making the best possible utilization of its converters. Due to limited laboratory resources, a small, low power prototype has been used for validation. It is expected that some advantages of the proposed scheme (e.g., high converter utilization, reduction in circulating power, enhanced stability due to turbine inertia, etc.) will be more pronounced for high-power PV-wind farm systems.

There is also a scope of designing the DFIG-wind turbine more optimally for the hybrid solution presented. The proposed hybrid combination can also render a neat stand-alone energy solution with minimum storage and can, in fact, be developed as a dispatchable source. Overall, the proposed system makes good use of the nature's complementary behavior for wind velocity and solar radiation. Sometimes this complementary trend may break down, in which case the proposed control scheme is well equipped to prevent converters' overloading at the cost of momentary loss of PV power. Such instances, however, are expected to be rare.

REFERENCES

1. J. Carrasco, L. Franquelo, J. Bialasiewicz, E. Galvan, R. Guisado, Ma. A. M. Prats, J. Leon, and N.Moreno-Alfonso, "Power-electronic systems for the grid integration of renewable energy sources: A survey," IEEE Trans. Ind. Electron., vol. 53, no. 4, pp. 1002–1016, Aug. 2006.
2. W. Kellogg, M. Nehrir, G. Venkataramanan, and V. Gerez, "Generation unit sizing and cost analysis for stand-alone wind, photovoltaic and hybrid wind/PV systems," IEEE Trans. EnergyConvers., vol. 13, no. 1, pp. 70–75, Mar. 1998.

3. S. Daniel and N. Ammasai Gounden, "A novel hybrid isolated generating system based on PV fed inverter-assisted wind-driven induction generators," IEEE Trans. Energy Convers., vol. 19, no. 2, pp. 416–422, Jun. 2004.
4. J. Yao, H. Li, Y. Liao, and Z. Chen, "An improved control strategy of limiting the DC-link voltage fluctuation for a doubly fed induction wind generator," IEEE Trans. Power Electron., vol. 23, no. 3, pp. 1205–1213, May 2008.
5. G. Tapia, A. Tapia, and J. Ostolaza, "Proportional-integral regulator-based approach to wind farm reactive power management for secondary voltage control," IEEE Trans. Energy Convers., vol. 22, no. 2, pp. 488–498, Jun. 2007.
6. J. Costa, H. Pinheiro, T. Degner, and G. Arnold, "Robust controller for DFIGs of grid-connected wind turbines," IEEE Trans. Ind. Electron., vol.58, no. 9, pp. 4023–4038, Sep. 2011.
7. C. Liu, F. Blaabjerg,W. Chen, and D. Xu, "Stator current harmonic control with resonant controller for doubly fed induction generator," IEEE Trans. Power Electron., vol. 27, no. 7, pp. 3207–3220, Jul. 2012.
8. H. Xu, J. Hu, and Y. He, "Operation of wind-turbine-driven DFIG systems under distorted grid voltage conditions: Analysis and experimental validations," IEEE Trans. Power Electron., vol. 27, no. 5, pp. 2354–2366, May 2012.
9. H. Nian and Y. Song, "Direct power control of doubly fed induction generator under distorted grid voltage," IEEE Trans. Power Electron., vol. 29, no. 2, pp. 894–905, Feb. 2014.
10. A. Yazdani, A. Di Fazio, H. Ghoddami,M. Russo,M. Kazerani, J. Jatskevich, K. Strunz, S. Leva, and J. Martinez, "Modeling guidelines and a benchmark for power system simulation studies of three-phase singlestage photovoltaic systems," IEEE Trans. Power Del., vol. 26, no. 2, pp. 1247–1264, Apr. 2011.
11. Z. Dejia, Z. Zhengming, M. Eltawil, and Y. Liqiang, "Design and control of a three-phase grid-connected photovoltaic system with developed maximum power point tracking," in Proc. Appl. Power Electron. Conf., Austin, Feb. 2008, pp. 973–979.
12. S. Eftekharnejad, V. Vittal, G. Heydt, B. Keel, and J. Loehr, "Impact of increased penetration of photovoltaic generation on power systems," IEEE Trans. Power Syst., vol. 28, no. 2, pp. 893–901, May 2013.
13. A. Canova, L. Giaccone, F. Spertino, and M. Tartaglia, "Electrical impact of photovoltaic plant in distributed network," IEEE Trans. Ind. Appl., vol. 24, no. 1, pp. 341–347, Feb. 2009.
14. M. Bouzguenda and S. Rahman, "Value analysis of intermittent generation sources from the system operations perspective," IEEE Trans. Energy Convers., vol. 3, no. 2, pp. 484–490, Sep. 1993.
15. Y. Chen, C. Cheng, and H. Wu, "Grid-connected hybrid PV/wind power generation system with improved DC bus voltage regulation strategy," in Proc. Appl. Power Electron. Conf. Expo., TX, Mar. 2006, pp. 1088–1094.
16. N. Jin and Y. Jin, "High efficiency solar wind inverter with hybrid DC DC converter," U.S. Patent 2012 0170325 A1, Jul. 5, 2012.
17. X. Tang,W. Deng, and Z. Qi, "A complementary power supply system of wind power generation and photovoltaic power generation based on supercapacitor batterymixing energy storage," Chinese PatentCN101309017A, Nov. 19, 2008.
18. F. Nejabatkhah, S. Danyali, S. Hosseini, M. Sabahi, and S. Niapour, "Modeling and control of a new three-input DC–DC boost converter for hybrid PV/FC/battery power system," IEEE Trans. Power Electron., vol. 27, no. 5, pp. 2309–905, Feb. 2014.
19. NREL Data. (2012, Jun. 1) [Online]. Available: http://www.nrel.gov/ midc/apps/daily.pl?site = BMS&start = 20080901&yr = 2012&mo = 8 &dy = 31